ORIGINAL ARTICLE

Grids of stellar models and frequencies with CLÉS + LOSC

**Josefina Montalbán · Andrea Miglio · Arlette Noels ·
Richard Scuflaire**

Abstract We present a grid of stellar models, obtained with the CLÉS evolutionary code, following the specification of ESTA-Task1, and the corresponding seismic properties, computed with the LOSC code. We provide a complete description of the corresponding files that will be available on the ESTA web-pages.

Keywords Stars: evolution · Stars: interiors · Stars: oscillations

PACS 97.10.Cv · 97.10.Sj · 95.80+p

1 Introduction

The preparation of the CoRoT mission brought up the need of a reference grid of stellar models in order to locate the possible CoRoT targets in the Hertzsprung–Russell (HR) diagram, and to allow a first interpretation of the forthcoming CoRoT-data. For this purpose, several grids of stellar models were computed according to the ESTA-Task1 specifications. In this paper we present the grids of stellar models we computed with the code CLÉS (Scuflaire et al. 2007a), as well

J. Montalbán (✉) · A. Miglio · A. Noels · R. Scuflaire
Institut d'Astrophysique et Géophysique, Université de Liège,
allée du 6 Août 17, 4000 Liège, Belgium
e-mail: j.montalban@ulg.ac.be

A. Miglio
e-mail: a.miglio@ulg.ac.be

A. Noels
e-mail: arlette.noels@ulg.ac.be

R. Scuflaire
e-mail: r.scuflaire@ulg.ac.be

as the seismic properties we derived by using the adiabatic oscillation code LOSC (Scuflaire et al. 2007b) for models on the main sequence (MS) or close to it.

In Sects. 2 and 3 we describe, respectively, the input physics and the set of stellar parameters we used. The evolutionary tracks, stellar models and oscillation frequency data can be found on the ESTA Web site. The description of all this material is given in Sect. 4 for the evolution and structure models, and in Sect. 5 for the seismic properties of the stellar models. Finally, in Sect. 6 we summarize the type and amount of available files.

2 Input physics

For three out of four stellar model grids we adopted the reference input physics, as well as the physical and astronomical constants specified for ESTA-Task1 comparisons (see also Sect. 5 in Morel and Lebreton 2007). We stress that these specifications do not always coincide with those of the standard version of CLÉS (see Scuflaire et al. 2007a).

– **Equation of State (EoS)**—OPAL2001 equation of State (Rogers and Nayfonov 2002) available in the OPAL Web site. The tabulated values of C_V have been replaced with the values derived from the tabulated values of P, Γ_1, χ_T, χ_ρ. For each ρ, T, X and Z we interpolate in the tables by using our own interpolation routine.
– **Opacities**—OPAL96 (Iglesias and Rogers 1996). The opacity tables used in CLÉS have been calculated on-line for the standard GN93 (Grevesse and Noels 1993) metal mixture, and using the smoothing routine available in the OPAL Web site to build the final opacity tables. The low temperature opacity tables by Alexander and Ferguson (1994) are also smoothly added (see Scuflaire et

al. 2007a), and conductive opacities were not included in these computations. As for EoS, we interpolate in ρ, T, X and Z by using our own interpolation routines.

– **Nuclear network**—We choose the same nuclear network as in model comparison, that is, basic pp chain and CNO cycle reactions up to the $^{17}O(p, \alpha)^{14}N$. We adopted the nuclear reaction rates from the analytical formulae provided by the NACRE compilation (Angulo et al. 1999), including that one for the $^{14}N(p, \gamma)^{15}O$, and the weak screening factors from Salpeter (1954). The electronic density, taking part in the screening factor computation, was estimated assuming full ionization of chemical elements.

– **Chemical composition**—We adopted the metal distribution provided by the Grevesse and Noels (1993) (thereafter GN93) solar mixture. Only the abundances of light elements (Li, Be and B) were modified to be consistent with those used in CESAM. The isotopic ratios are those of Anders and Grevesse (1989) except for the $^{2}H/^{1}H$ and $^{3}He/^{4}He$ ratios for which we took those of Gautier and Morel (1997).

– **Convection**—All the evolutionary tracks were computed with the classical mixing length treatment of convection by Böhm-Vitense (1958) and the formulation of Henyey et al. (1965) for optically thin regions. The mixing length parameter α_{MLT} was fixed at 1.6 for all the grids. Note that the latter is the value chosen for ESTA comparisons, but it does not correspond to the value derived from a solar calibration.

– **Overshooting.** All the models, regardless of their mass, were computed without convective core overshooting.

– **Atmosphere.** ESTA-Task1 specification requires the surface boundary conditions to be provided by integration of a grey atmosphere following the Eddington's $T(\tau)$ law (grey models, thereafter). Three of the four stellar model grids were computed following the ESTA specification, while for the fourth one, temperature and density at $T = T_{eff}$ were obtained from Kurucz's atmosphere models (Kurucz 1998).

3 Stellar parameters

We provide evolutionary tracks for masses from 0.8 to $8M_{\odot}$, with a mass step $\Delta M = 0.1$, from 0.8 to $1.6M_{\odot}$, $\Delta M = 0.2$ up to $4.0M_{\odot}$, and $\Delta M = 0.5$ from 4.0 to $8.0M_{\odot}$.

The initial hydrogen mass fraction is $X = 0.70$ in all grids. Three different values of the metal mass fraction Z (0.02, 0.01 and 0.006) are available for grids of grey models, while only $Z = 0.02$ has been considered in the grid computed with Kurucz atmosphere boundary conditions.

4 Data

4.1 Evolutionary tracks

For each stellar parameter (M, X, Z) we follow the PMS evolution from the Hayashi track, and the calculation ends either when the temperature at the stellar center is high enough to burn He, or when the age of the model is larger than 20 Gyr. We recall that the computation of these models does not include conductive opacities and that these ones should be taken into account in modeling low mass stars up to the helium ignition. The grids of these evolutionary tracks are available from the ESTA Web site[1] and consist of **two** HRD-files, whose name contains the values of the stellar parameters for which they were computed. For instance, "m1.00Z0.02X0.70-HRD1.txt" and "m1.00Z0.02X0.70-HRD2.txt" contain the evolutionary tracks for a $1.00M_{\odot}$ star with initial chemical composition $X = 0.70$ and $Z = 0.02$. The first four lines in HRD1 and HRD2-files provide information about the stellar parameters and the input physics used to build the model. Since most of them have already been described in previous section, we only mention that **fg** and **ft** indicate the factor by which the mesh and time step were multiplied. Both, fg and ft were set equal to 0.5, that is, the number of mesh points and the temporal steps were doubled with respect to the standard value used in CLÉS (Scuflaire et al. 2007b). The quantities for which the temporal evolution were tabulated in the HRDs files are the following:

HRD1 files:

– **Column 1**—Stellar mass in units of $M_{\odot}$.
– **Column 2**—Stellar luminosity ($\log(L/L_{\odot})$).
– **Column 3**—Decimal logarithm of the effective temperature in K ($\log T_{eff}$).
– **Column 4**—Stellar radius in units of solar radius ($R/R_{\odot}$).
– **Column 5**—Stellar age in Myr.
– **Column 6**—Hydrogen mass fraction at the center.
– **Column 7**—$\log g$, with g, the surface gravity.
– **Column 8**—Number of convective-radiative boundaries.
– **Column 9**—Codification of the of boundary type: "2" for boundary from convective to radiative region; and "1" for boundaries from radiative to convective one, going from the stellar center towards the surface.
– **Column 10–15**—Relative radius of the six first convective-radiative boundaries (from the center outwards).

HRD2 files:

– **Column 1**—Number of model.
– **Column 2**—Stellar age in Myr.
– **Column 3**—Stellar radius in solar radius ($R/R_{\odot}$).

---

[1]http://www.astro.up.pt/corot/models

Fig. 1 Theoretical HR diagram for the evolution phase comprised between the initial homogeneous model and that with a hydrogen mass fraction at the center reduced by 1% with respect to the initial model (that is, $X_c = 0.693$). Evolutionary tracks are labeled by the corresponding stellar mass. *Solid lines* correspond to grey models and *dashed* ones to models with Kurucz boundary conditions
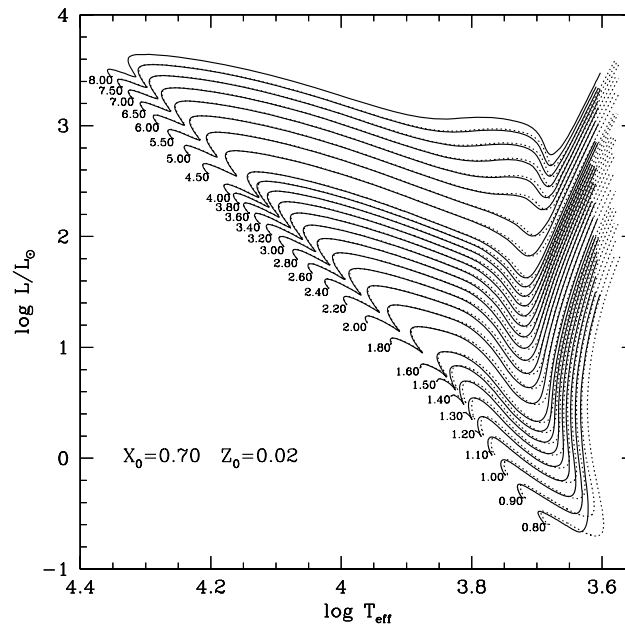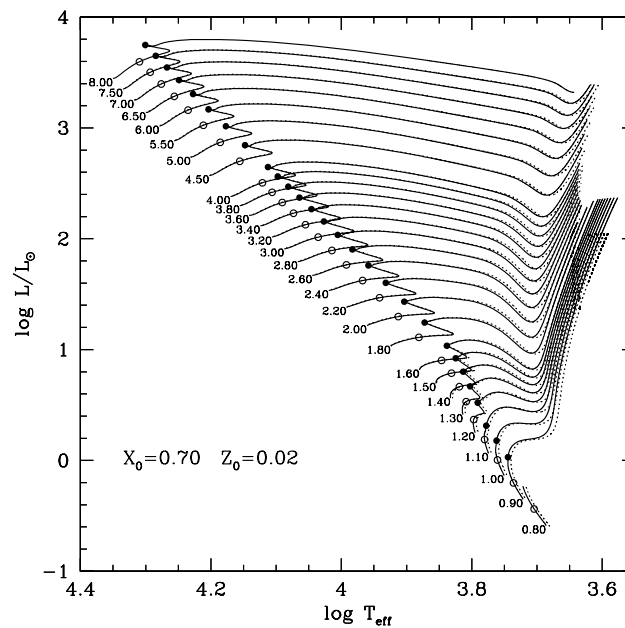
Fig. 2 As Fig. 1 for the evolutionary phase of main sequence and post-main sequence. *Open circles* indicate the location of models that has burned, at the center, half of the initial hydrogen. *Solid circles* correspond to models with only 0.1% of hydrogen at the center

– **Column 4**—Stellar luminosity in units of solar luminosity ($L/L_\odot$).
– **Column 5**—Effective temperature in K.
– **Column 6**—Temperature at the center in units of 10^7 K.
– **Column 7**—Central density ρ_c in g cm^{-3}.
– **Column 8**—Hydrogen mass fraction at the center (X_c).
– **Column 9**—Central helium mass fraction (Y_c).
– **Column 10**—Number of convective regions.
– **Column 11**—Relative mass of the convective core (m_{cc}/M_*).
– **Column 12**—Relative radius of the base of the outer convective region (R_{ce}/R_*).

– **Column 13**—Mass of the helium core in $M_\odot$. The helium core is defined by the mass of the region with a hydrogen mass fraction smaller than 10^{-2}.

The $\log T_{eff}$–$\log L/L_\odot$ diagram for all the models with a metal mass fraction $Z = 0.02$ have been plotted in Fig. 1 for the PMS evolution, and in Fig. 2 for the MS and Post-MS evolutionary phases. For each mass there is a pair of curves, one was computed with Eddington's law as boundary conditions at the photosphere (solid lines) and the other used Kurucz's atmosphere models (dashed lines). It is interesting to note that, as it concerns the theoretical HR diagram, the atmosphere type affects only models with effective tempera-
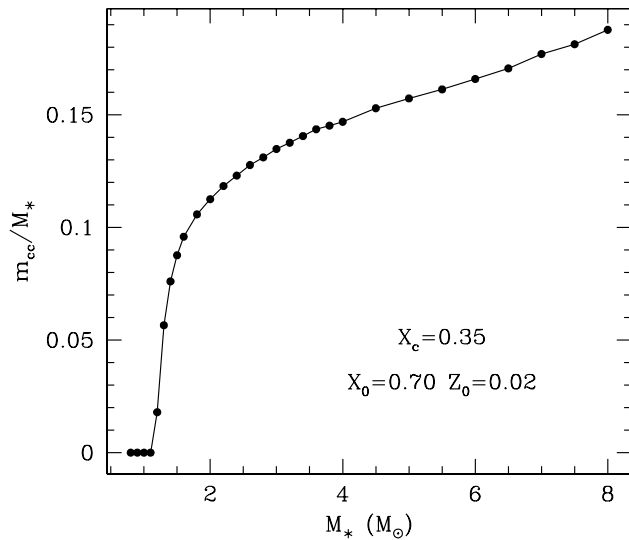
Fig. 3 Relative mass of the convective core as a function of the stellar mass for models that have burned the half of their initial H content at the center
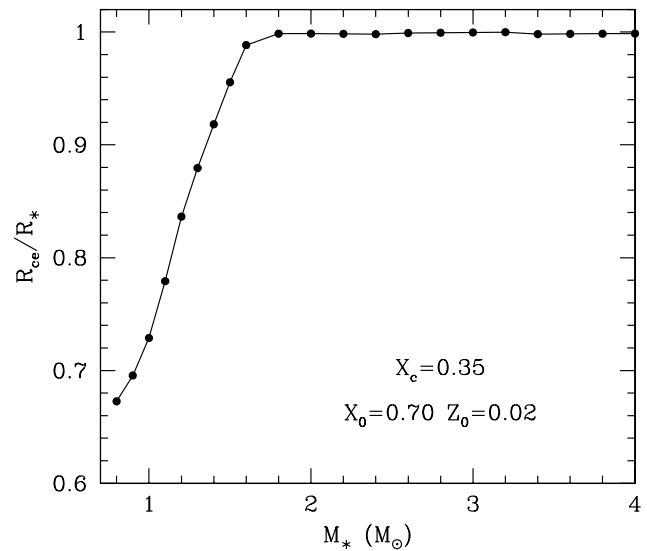

Fig. 4 Relative radius of the outer envelope bottom as a function of the stellar mass for the same models as in Fig. 3

ture lower than 6300 K. The effects on the seismic properties will be discussed in Sect. 5.

In Fig. 2 we marked the model locations at the middle of their MS (central hydrogen mass fraction $X_c = 0.35$) by open circles and that of models with a central hydrogen mass fraction $X_c \simeq 0.001$ by filled ones. Defining the beginning of MS by the model with a central mass fraction of hydrogen decreased by 1% with respect to the initial one (that is $X_c = 0.693$ for the present computations), and its end by that with $X_c \simeq 0.001$, the MS-lifetime varies from 5×10^7 yrs for $8 M_\odot$ to more than 13 Gyr for $0.9 M_\odot$. The number of computed stellar models that span the main sequence phase of evolution is of the order of 160 for each (M, X, Z).

The dependence on the stellar mass of the convective core mass, for models in the middle of MS is shown in Fig. 3, and that of the convective envelope bottom in Fig. 4. Finally, in Fig. 5 we show the mass of the He core at the end of the MS as a function of the stellar mass.

4.2 Stellar models

In addition to the evolutionary tracks, a selection of internal structure models for each (M, X, Z) are also available:

– **ZAMS** model—defined as the model for which the ratio of gravitational to nuclear luminosity is lower than 2%.
– **1MS** model—as the model which has burned 1% of H ($X_c \simeq 0.693$).
– **MS** model—as the model with half of the initial H at the center ($X_c \simeq 0.35$).
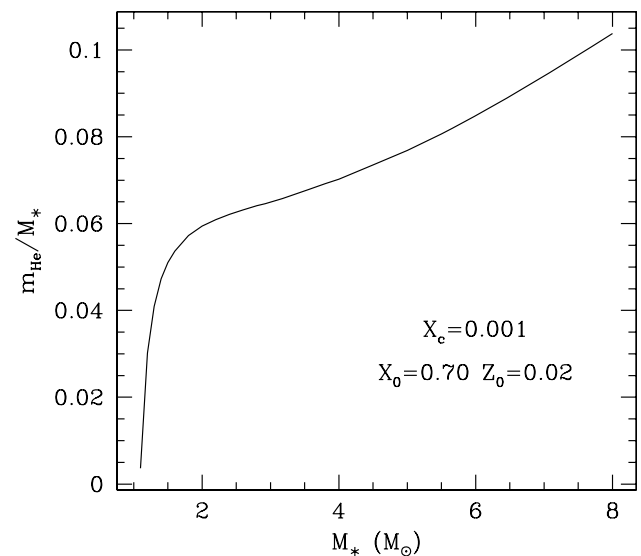– **TAMS** model—as the model with $X_c \simeq 0.01$.

Fig. 5 Relative mass of the helium core at the end of the MS phase as a function of the stellar mass

– One every five models spanning the MS phase of evolution: from $X_c = 0.693$ to $X_c = 0.001$. That means about 30 models for each set of stellar parameters.

An individual file is provided for each stellar model whose name is formed with the stellar parameters, for example: m1.00Z0.02X0.70-####.gong, where "####" can be "ZAMS", "1MS", "MS", "TAMS", or a number corresponding to the number of the model. The format adopted for these

files is the **FGONG**[2] one with the first twenty-five variables. The number of mesh points through the stellar interior is of the order of 2200, and 100 additional mesh points are used to describe the stellar atmosphere from an optical depth $\tau = 2/3$ outwards, up to $\tau = 10^{-3}$.

Among the physical quantities stored in **FGONG** files there are the mass fraction of the most important contributors to nuclear energy generation. For illustration, we show in Fig. 6 the chemical profile of key elements such as ^{3}He, ^{12}C, and ^{14}N inside the stellar models in the mid-MS.

5 Seismic properties

For each equilibrium model in FGONG format, we also provide a file containing the properties of radial and non radial oscillation modes with spherical degree $\ell = 1, 2,$ and 3. These properties were computed by using the code LOSC (Scuflaire et al. 2007b) with the standard surface boundary condition (regularity of solution when $P = 0$ at the surface, that is, $\delta P/P + (4 + \omega^2)\delta r/r = 0$). The angular frequencies of the computed oscillation modes cover the domain given by 0.3–50 times the dynamical time ($\tau_{\text{dym}} = \sqrt{R^3/G M}$).

The file name is the same as that of the equilibrium model but with the extension ".freq"; the content is the following:

– **Column 1**—spherical angular degree ℓ.
– **Column 2**—radial order n.
– **Column 3**—dimensionless frequency $\omega = \sigma \cdot \tau_{\text{dym}}$.
– **Column 4**—angular frequency σ.
– **Column 5**—frequency $\nu = \sigma/2\pi$ in Hz.
– **Column 6**—period P in seconds.
– **Column 7**—$\beta_{n\ell} = 1 - C_{n\ell}$ gives the frequency shift generated by solid rotation, where $C_{n\ell}$ is the Ledoux's constant (Ledoux 1951).
– **Column 8** — fraction of the kinetic energy associated to the radial component of the motion $ev = E_{\text{kin,V}}/E_{\text{kin}}$.
– **Column 9**—$x_m = \langle x \rangle$ is the mean value of $x = r/R$ weighted by the kinetic energy of the oscillation mode, and determines in which region the mode is trapped.
– **Column 10**—$\Delta = 2\sqrt{\langle x^2 \rangle - \langle x \rangle^2}$, that takes values between 0 and 1, vanishes for a perfectly trapped mode.

Since discontinuities in the sound speed derivatives in the stellar interior (such as those introduced by the boundaries of the convective regions and by the second helium ionization zone) produce periodic signatures in the frequencies of low degree modes (see e.g. Gough 1990), we decided to provide, as well, files containing the time variations of some quantities that may be of interest in the seismic analysis of stellar models. So, for each stellar parameter set (M, X, Z),
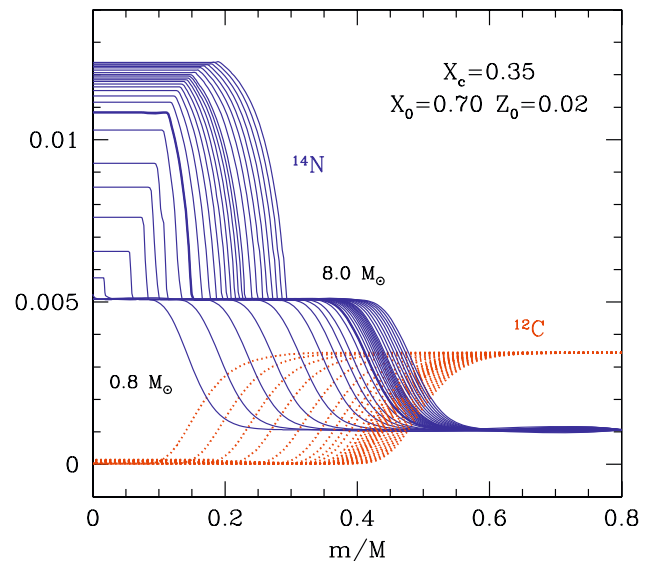
Fig. 6 Upper panel: equilibrium abundance of ^{3}He for models with masses from 0.8 to $8M_\odot$. Lower panel: equilibrium abundance of ^{14}N (*solid lines*) and ^{12}C (*dotted lines*) for each of the considered stellar masses. The thicker lines correspond to the chemical profile in a $2M_\odot$ model

but only for the MS-lifetime, we built a file whose name is formed, as for HR diagram ones, with the values of the stellar parameters (for instance "m1.00Z0.02X0.70-ACC.txt"), and whose content in the columns 7–13 is the following:

– **Cutoff frequency** (in μHz) at the photosphere (column 7): $\nu_{\text{ac}} = c/(4\pi H_p)$ where c is the sound speed, and H_p the pressure scale height.
– **Acoustic radius** in seconds (column 8): $r_{\text{ac}} = \int_0^R 1/c \, dr$ where R is the stellar radius at the photosphere.
– **Acoustic depth** in seconds of the border of the convective core (column 10) corresponding to the linear relative radius r_{cc}/R given in column 9.
– **Acoustic depth** in seconds of the bottom of the convective envelope (column 12) corresponding to the linear relative radius r_{ce}/R given in column 11.
– **Second He ionization region**: linear relative radius (r_{HeII}/R) in column 12, and the corresponding acoustic depth τ_{HeII} in column 13.

The four first lines, and the columns 1–6 are the same as in HRD2-files.

In principle, only oscillation modes with frequencies lower than the acoustic cutoff one are trapped in the stellar interior and should be observed. As an indication of the order of magnitude of the expected oscillation frequencies we show in Fig. 7 the variation with time of the cutoff frequency for models with masses smaller than $2M_\odot$.
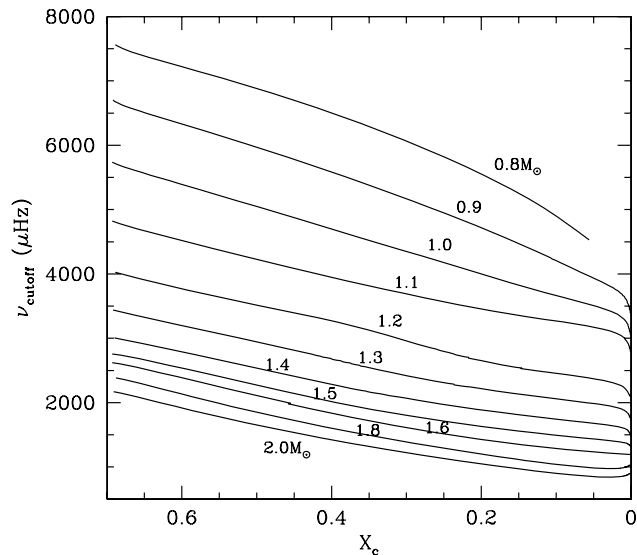
Fig. 7 Evolution of the cutoff frequency along the MS evolution of models with masses from $0.8M_\odot$ (*upper curve*) to $2M_\odot$ (*lower curve*)

Fig. 8 Difference between the oscillation frequencies of $1.8M_\odot$ models computed with Eddington's grey law (ν_E) and with Kurucz's atmospheres (ν_K)

5.1 Effect of atmospheric boundary conditions

For the chemical composition $X = 0.70$ and $Z = 0.02$ there are two types of stellar models depending on whether the boundary conditions at $T = T_{eff}$ are given by Kurucz atmosphere models or by grey ones (with Eddington's law). We showed in Figs. 1 and 2 that the effect on the HRD location was significant only for $T_{eff} \lessapprox 6300$ K. The effect on the oscillation frequencies may be, however, important even for higher temperatures. As an example we show in Fig. 8 the difference between oscillation frequencies for $1.8M_\odot$ models in mid-MS. The difference in the global parameters for these Eddington and Kurucz stellar models are $\Delta R/R = 4 \times 10^{-4}$, $\Delta L/L = 1.4 \times 10^{-5}$, and $\Delta X_c < 10^{-5}$. Nevertheless, the density at $T = T_{eff}$ provided by the two atmosphere models is different enough to affect a significant fraction of the star, leading to an important variation of the oscillation frequencies. Note that for this comparison only the subphotospheric stellar structure was considered in the computation of the oscillation frequencies. The differences at high frequency will be even larger if the atmosphere structure is included in the calculation.

6 Conclusions

In order to provide a reference grid of stellar models for the first interpretation of the CoRoT data, we have computed three sets of grey stellar models for 29 different masses from 0.8 to $8M_\odot$. Each grid is computed with a different chemical composition, and altogether they span metallicity values from $[M/H] = -0.45$ to $+0.07$ (taking as reference the
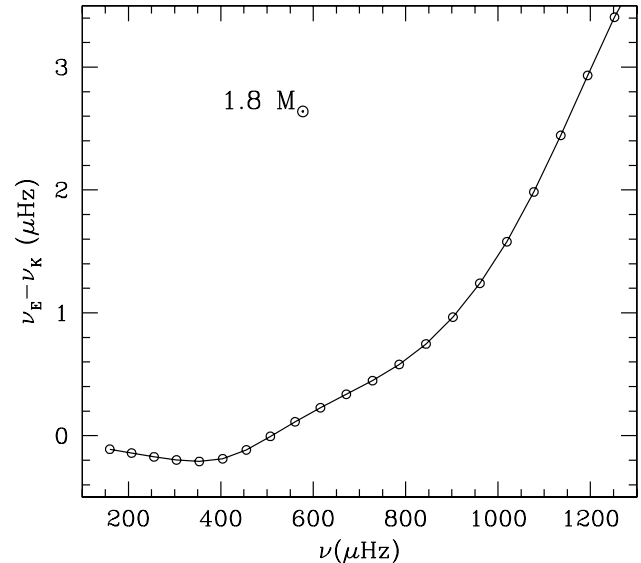
value of $Z/X = 0.0245$ for the Sun given by GN93). There are $3 \times 29 \times 3 = 261$ files containing data on time evolution of global quantities, around 3050 files with the detailed stellar structure (interior and atmosphere), and other 3050 with the corresponding oscillation frequencies for low degree modes ($\ell = 0$, 1, 2, and 3). In addition, a set of stellar models with the Kurucz's atmospheres as boundary conditions were also computed, for the same values of stellar mass, but for only one chemical composition. That means additional ∼2087 files, 87 for the time evolution, and the rest of them for the stellar structure and the corresponding seismic properties.

References

Alexander, D.R., Ferguson, J.W.: Low-temperature Rosseland opacities. Astrophys. J. **437**, 879–891 (1994). doi:10.1086/175039

Anders, E., Grevesse, N.: Abundances of the elements—meteoritic and solar. Geochim. Cosmochim. Acta **53**, 197–214 (1989). doi:10.1016/0016-7037(89)90286-X

Angulo, C., Arnould, M., Rayet, M., Descouvemont, P., Baye, D., Leclercq-Willain, C., Coc, A., Barhoumi, S., Aguer, P., Rolfs, C., Kunz, R., Hammer, J.W., Mayer, A., Paradellis, T., Kossionides, S., Chronidou, C., Spyrou, K., degl'Innocenti, S., Fiorentini, G., Ricci, B., Zavatarelli, S., Providencia, C., Wolters, H., Soares, J., Grama, C., Rahighi, J., Shotter, A., Lamehi Rachti, M.: A compilation of charged-particle induced thermonuclear reaction rates. Nucl. Phys. A **656**, 3–183 (1999)

Böhm-Vitense, E.: Über die Wasserstoffkonvektionszone in Sternen verschiedener Effektivtemperaturen und Leuchtkräfte. Mit 5 Textabbildungen. Z. Astrophys. **46**, 108 (1958)

Gautier, D., Morel, P.: A reestimate of the protosolar $(^2H/^1H)_p$ ratio from $(^3He/^4He)_{SW}$ solar wind measurements. Astron. Astrophys. **323**, L9–L12 (1997)

Grevesse, N., Noels, A.: Cosmic abundances of the elements. In: Origin and Evolution of the Elements. Cambridge University Press, Cambridge (1993)

Gough, D.O.: Comments on helioseismic inference. In: Osaki, Y., Shibahashi, H. (eds.) Progress of Seismology of the Sun and Stars. Lecture Notes in Physics, vol. 367, pp. 283–318. Springer, Berlin (1990). doi:10.1007/3-540-53091-6_93

Henyey, L., Vardya, M.S., Bodenheimer, P.: Studies in stellar evolution. III. The calculation of model envelopes. Astrophys. J. **142**, 841 (1965)

Iglesias, C.A., Rogers, F.J.: Updated opal opacities. Astrophys. J. **464**, 943 (1996)

Kurucz, R.L.: Grids of model atmospheres. http://kurucz.harvard.edu/grids.html (1998)

Ledoux, P.: The nonradial oscillations of gaseous stars and the problem of beta canis majoris. Astrophys. J. **114**, 373 (1951)

Morel, P., Lebreton, Y.: CESAM: a free code for stellar evolution calculations. Astrophys. Space Sci. (2007). doi:10.1007/s10509-007-9663-9

Rogers, F.J., Nayfonov, A.: Updated and expanded OPAL equation-of-state tables: implications for helioseismology. Astrophys. J. **576**, 1064–1074 (2002). doi:10.1086/341894

Salpeter, E.E.: Electrons screening and thermonuclear reactions. Aust. J. Phys. **7**, 373 (1954)

Scuflaire, R., Théado, S., Montalbán, J., Miglio, A., Bourge, P.-O., Godart, M., Thoul, A., Noels, A.: CLÉS, Code Liégeois d'Évolution Stellaire. Astrophys. Space Sci. (2007a). doi:10.1007/s10509-007-9650-1

Scuflaire, R., Montalbán, J., Théado, S., Bourge, P.O., Miglio, A., Godart, M., Thoul, A., Noels, A.: The Liège OScillations Code. Astrophys. Space Sci. (2007b) doi:10.1007/s10509-007-9577-6